

PREPRINT SUBMITTED

This manuscript is a preprint uploaded to EarthArXiv, not yet peer-reviewed. This preprint was submitted for publication to *Geochemistry, Geophysics, Geosystems* in March 2024, re-submitted to *Earth Surface Dynamics* in May 2024, and its revision (this version) submitted January 31st 2025. Authors encourage downloading the latest manuscript version from EarthArXiv, and welcome comments, feedback and discussions anytime. Please, feel free to get in contact with the first author: gino.de-gelder@univ-grenoble-alpes.fr

Bayesian reconstruction of sea-level and hydroclimates from coastal landform inversion: application to Santa Cruz (US) and Gulf of Corinth

Gino de Gelder^{1,2,3}, Navid Hedjazian³, Laurent Husson¹, Thomas Bodin⁴, Anne-Morwenn Pastier⁵, Yannick Boucharat¹, Kevin Podoja⁶, Tubagus Solihuddin², Sri Y. Cahyarini²

¹ISTerre, IRD, CNRS, Université Grenoble-Alpes, Saint-Martin d'Hères, 38400, France

²Res. Group of Paleoclimate & Paleoenvironment, Res. Centr. for Climate and Atmosphere, Res. Org. of Earth Sciences and Maritime, National Research and Innovation Agency, Bandung, 40135, Indonesia

³ENS de Lyon, CNRS, LGL-TPE, Université Claude Bernard Lyon1, Villeurbanne, 69100, France

⁴Instituto de Ciencias del Mar (ICM) - CSIC, Barcelona, Spain

⁵GeoForschungsZentrum, Potsdam, 14473, Germany

⁶Université de Caen Normandie, Caen, 14000, France

Correspondence to: Gino de Gelder (gino.de-gelder@univ-grenoble-alpes.fr)

1 Bayesian reconstruction of sea-level and hydroclimates from 2 coastal landform inversion: application to Santa Cruz (US) and 3 Gulf of Corinth

4 Gino de Gelder^{1,2,3}, Navid Hedjazian³, Laurent Husson¹, Thomas Bodin⁴, Anne-Morwenn Pastier⁵,
5 Yannick Boucharat¹, Kevin Pedoja⁶, Tubagus Solihuddin², Sri Y. Cahyarini²

6 ¹ISTerre, IRD, CNRS, Université Grenoble-Alpes, Saint-Martin d'Hères, 38400, France

7 ²Res. Group of Paleoclimate & Paleoenvironment, Res. Centr. for Climate and Atmosphere, Res. Org. of Earth
8 Sciences and Maritime, National Research and Innovation Agency, Bandung, 40135, Indonesia

9 ³ENS de Lyon, CNRS, LGL-TPE, Université Claude Bernard Lyon1, Villeurbanne, 69100, France

10 ⁴Instituto de Ciencias del Mar (ICM) - CSIC, Barcelona, Spain

11 ⁵GeoForschungsZentrum, Potsdam, 14473, Germany

12 ⁶Université de Caen Normandie, Caen, 14000, France

13 *Correspondence to:* Gino de Gelder (gino.de-gelder@univ-grenoble-alpes.fr)

14 **Abstract.** Quantifying Quaternary sea-level changes and hydroclimatic conditions is an important challenge given
15 their intricate relation with paleo-climate, ice-sheets and geodynamics. The world's coastlines provide an enormous
16 geomorphologic archive, from which forward landscape evolution modelling studies have shown their potential to
17 unravel paleo sea-levels, albeit at the cost of assumptions to the genesis of these landforms. We take a next step, by
18 applying a Bayesian approach to jointly invert the geometries of multiple coastal terrace sequences to paleo sea- and
19 lake level variations and extract past hydroclimatic conditions. Using a Markov chain Monte Carlo sampling method,
20 we first test our approach on synthetic marine terrace profiles as proof of concept and benchmark our model on an
21 observed marine terrace sequence in Santa Cruz (US). We successfully reproduce observed sequence morphologies
22 and simultaneously obtain probabilistic estimates for past sea-level variations, as well as for other model parameters
23 such as uplift and erosion rates. When applied to the semi-isolated Gulf of Corinth (Greece), our method allows
24 deciphering the geomorphic Rosetta stone at an unprecedented resolution, revealing the connectivity between the
25 Lake/Gulf of Corinth and the open sea for different hydroclimatic conditions. Eustatic sea-level and changing sill
26 depths drive marine and transitional phases during interglacial and interstadial periods, whereas wetter and drier
27 hydroclimates respectively over- and under-fill Lake Corinth during interstadial and glacial periods.

28 **Short summary.** Marine terrace sequences - staircase-shaped coastal landforms - record sea-level changes, vertical
29 motions and erosional processes that are difficult to untangle. To do so we developed a numerical inversion approach:
30 using the observed landscape as input, we constrain the ensemble of parameter ranges that could have created this
31 landscape. We apply the model to marine terrace sequences in Santa Cruz (US) and Corinth (Greece) to reveal past
32 sea/lake levels, uplift rates and hydro-climates.

33 1 Introduction

34 Reconstructions of Quaternary sea-level variations provide crucial constraints on thresholds and feedbacks within
35 climatic and geodynamic systems that help understand how contemporary climate change may affect future sea level
36 (Lambeck and Chappell, 2001; Hay et al., 2014; Dutton et al., 2015; Shakun et al., 2015; Austermann et al., 2017). A
37 key archive of past sea-level is exposed within the geomorphology of most of the world's coastal areas in the form of
38 paleo-shorelines (Johnson and Libbey, 1997; Pedoja et al., 2011, 2014; Rovere et al., 2023; Fig. 1a), but it remains
39 difficult to accurately translate coastal observations and measurements into paleo-sea-level estimates, and to evaluate
40 the uncertainties inherent to these conversions. Major challenges include 1) dating of these landforms, as most paleo-

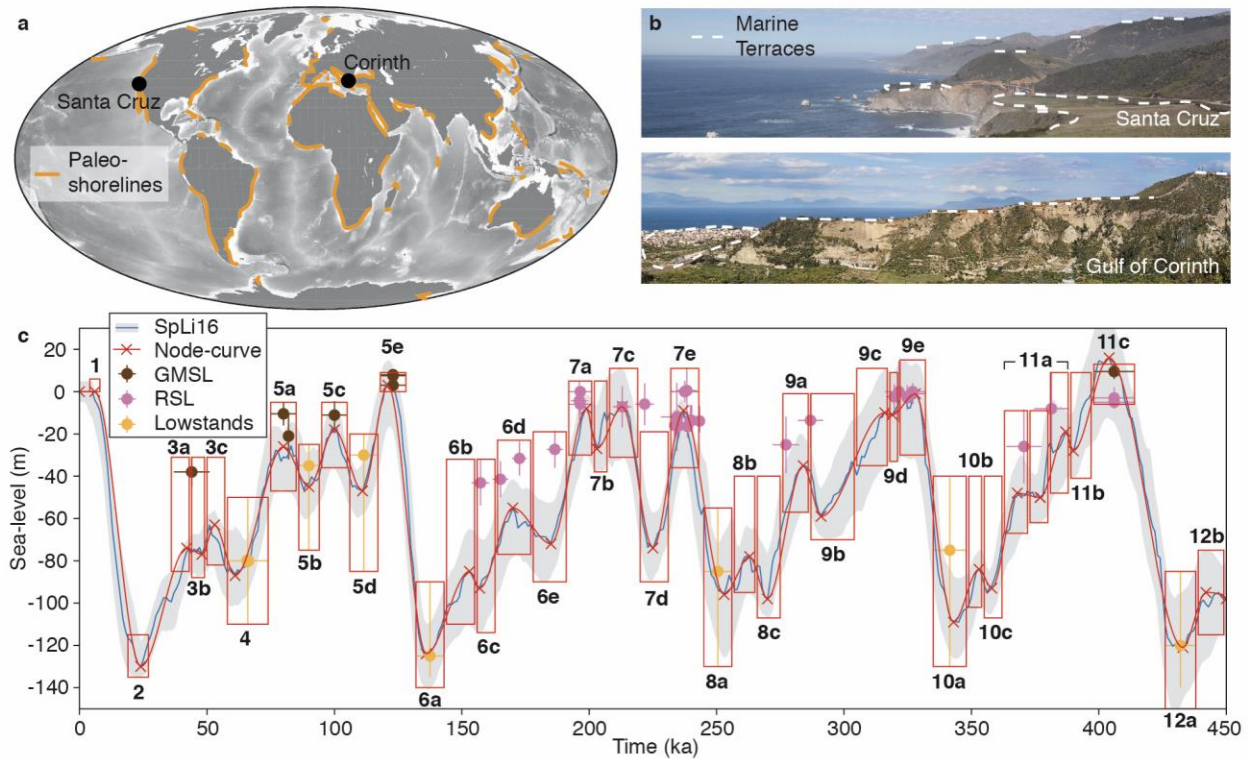
41 shorelines are erosive in nature (Pedoja et al., 2014) and absolute dating techniques themselves are complex and prone
42 to large uncertainties (Strobl et al., 2014; Hibbert et al., 2016; Ott et al., 2019), 2) observational bias, which are mostly
43 restricted to the most recent glacial cycle(s) and to periods where relative sea level was at similar elevations to present-
44 day (Medina-Elizalde, 2013; Hibbert et al., 2016), 3) absence of reciprocity between paleo-shorelines and sea-level
45 stands, as not all highstands lead to paleo-shorelines, and paleo-shorelines may have formed during one or many sea-
46 level cycles (Guilcher, 1974; Malatesta et al., 2021; Chauveau et al., 2023), and 4) separating the tectonic from the
47 sea-level component within relative sea-level changes (Pedoja et al., 2011).

48 Numerical models of landscape evolution started to overcome some of these limitations, by providing a means to
49 quantitatively interpret undated paleo-shorelines, incorporate full sea-level curves instead of highstands only,
50 unravelling the creation of paleo-shorelines formed over multiple glacial cycles, and considering multiple sea-level
51 curves (e.g. Webster et al., 2007; Jara-Muñoz et al., 2019; Leclerc and Feuillet, 2019; De Gelder et al., 2020; 2023).
52 So far, such numerical models have mainly been used for forward modelling approaches, where a number of proposed
53 sea-level curves are used to predict shorelines, which are then compared to actual observations. However, this only
54 provides a limited way to explore the full ensemble of possible sea-level histories and other model parameters like
55 rock erosion rates or effective wave base depths, which are difficult to estimate. It follows that uncertainties in sea-
56 level estimates from marine terraces remain poorly known, regardless of the method used, and in spite of
57 uniformization attempts (Lorscheid and Rovere, 2019).

58 Semi-isolated marine basins, i.e. bodies of water that have been connected to the open sea in some intervals of their
59 geologic history, and little or disconnected from the sea in other intervals, develop in hydrodynamic settings for which
60 it is particularly complex to reconstruct sea and lake level. Such basins, like the Red Sea, Sea of Marmara (Turkey),
61 Carioco Basin (Venezuela) and Gulf of Corinth (Greece), have a special geologic interest, given the active tectono-
62 sedimentary processes driving their formation (e.g. Van Daele et al., 2011; McNeill et al., 2019), their sensitivity to
63 rapid sea-level and climatic changes (e.g. Aksu et al., 1999; Siddall et al., 2004), and their role in dispersion of species
64 (e.g. Derricourt, 2005). The main complexity in reconstructing sea-/lake-level fluctuations in such settings, is that 1)
65 during disconnected phases these basins may have been underfilled or overfilled depending on local hydroclimate,
66 and 2) the structural highs (sills) separating the basins from the sea can be simultaneously affected by tectonic vertical
67 motion, sedimentation and erosion.

68 In this study, we intend to overcome common marine terrace analysis limitations, by using a Bayesian approach to
69 invert the geometry of paleo-shoreline sequences. Our approach provides probabilistic estimates of paleo sea-level,
70 erosion rates, uplift rates, wave-based depths and initial slopes. We focus on erosive marine terraces (Fig. 1b), which
71 are both the most common type of paleo-shoreline (Pedoja et al., 2014), and are simpler to model than their
72 depositional and bio-constructed equivalents (e.g. Pastier et al., 2019). We first apply our probabilistic inversion
73 approach to a set of synthetic coastal profiles to test and illustrate the method, after which we invert a well-studied
74 marine terrace sequence in Santa Cruz (US) to benchmark our model on a natural example. Finally, we use our
75 approach on the semi-isolated Gulf of Corinth to decipher the complex combination of tectonic uplift, sea- and lake-
76 level fluctuations, local climatic drivers and sill dynamics. The Gulf of Corinth has been considered as a natural rift
77 laboratory and has therefore received a lot of attention as a primary example for studying tectonic and surface
78 processes in young rift systems (e.g. Armijo et al., 1996; Bernard et al., 2006; Nixon et al., 2016, Gallen & Fernández-
79 Blanco, 2021). As a semi-isolated marine basin it has also been subjected to many studies on its environmental and
80 climatic evolution (e.g. Collier et al., 2000; Watkins et al., 2019), yet, so far, previous studies could not resolve to
81 what extent sea and lake levels have fluctuated.

82 These case studies highlight how we can derive probabilistic estimates of past sea-level from marine terraces, and how
83 the natural archive of paleo-shorelines can be further utilized to improve both paleo sea-level estimates, and unravel
84 complex tectono-hydro-climatic interactions.



86
 87 **Figure 1. Paleo-shorelines and paleo-sea level.** **a)** Global compilation of paleoshoreline sequences, adjusted from Pedoja et al.,
 88 2014, **b)** pictures of marine terrace sequences from Santa Cruz (US) and the Corinth Rift (Greece) and **c)** paleo-sea-level estimates
 89 for the past 450 ka, showing a sea-level curve (SpLi16, blue; Spratt and Lisiecki, 2016) derived from principal component analysis
 90 of 7 sea-level curves with its 2.5% and 97.5% likelihood range (grey envelope), an approximation of that curve with nodes and a
 91 cubic spline interpolation (red), global mean sea-level highstand estimates adjusted for glacio-istostatic adjustments (GMSL, brown
 92 dots; Kopp et al., 2009; Dutton et al., 2015; Pico et al., 2016; Creveling et al., 2017; Dyer et al., 2021; Tawil-Morsink et al., 2022),
 93 selected relative sea-level highstand estimates >130 ka (RSL, pink dots; Stirling et al., 2001; Murray-Wallace, 2002; Andersen et
 94 al., 2010; de Gelder et al., 2022; Marra et al., 2023), global mean sea-level lowstand estimates from ice sheet data (orange dots;
 95 Batchelor et al., 2019), and red boxes that represent the likely admissible range of relative sea-level elevations at locations far from
 96 the major ice-sheets (details in Supplementary Information and Table S1) that we consider in this study. Marine Isotope Stages
 97 (MIS) are given in bold, and based on Railsback et al., 2015.

98 2 Marine terrace sequence inversion

99 Marine terraces are relatively flat surfaces of coastal origin, either horizontal or gently inclined seawards (Fig 1b;
 100 Pirazzoli, 2005). They are bounded inland by a fossil sea-cliff, and can be covered by a layer of coastal sediments.
 101 Here we model erosive marine terraces, which are primarily formed by sea-cliff retreat in response to wave action.
 102 The superposition of Quaternary sea-level variations (Fig. 1c) and vertical land movement typically leads to a staircase
 103 landscape exhibiting marine terraces sequences (Fig. 1b).

104 The landscape evolution model we use (the code 'REEF'; Husson et al., 2018; Pastier et al., 2019) has a wave erosion
 105 module based on the wave energy dissipation model developed by Anderson et al. (1999). The model assumes that
 106 the vertical seabed erosion rate is a linear function of the rate of wave energy dissipation against the seabed (Sunamura,
 107 1992). Horizontal erosion rates depend on the energy available at the sea-cliff after dissipation of the far-field wave
 108 energy (Anderson et al., 1999). The dissipation rate is dictated by the water depth profile, which increases landwards
 109 exponentially with decreasing water depth. The initial erosion rate ER is expressed as an effective eroded volume per
 110 unit of time and coastal length, in which a fraction of erosional residual power ER_r erodes the foundation at each

111 location along the profile. This fraction ER_r depends on the water level, h , the water depth for wave base erosion WB ,
112 and a coefficient for sea bed erodibility K , so that:

$$\frac{dER_r}{dt} = K \times ER_r \times \exp\left(-\frac{h}{WB}\right) \quad (1)$$

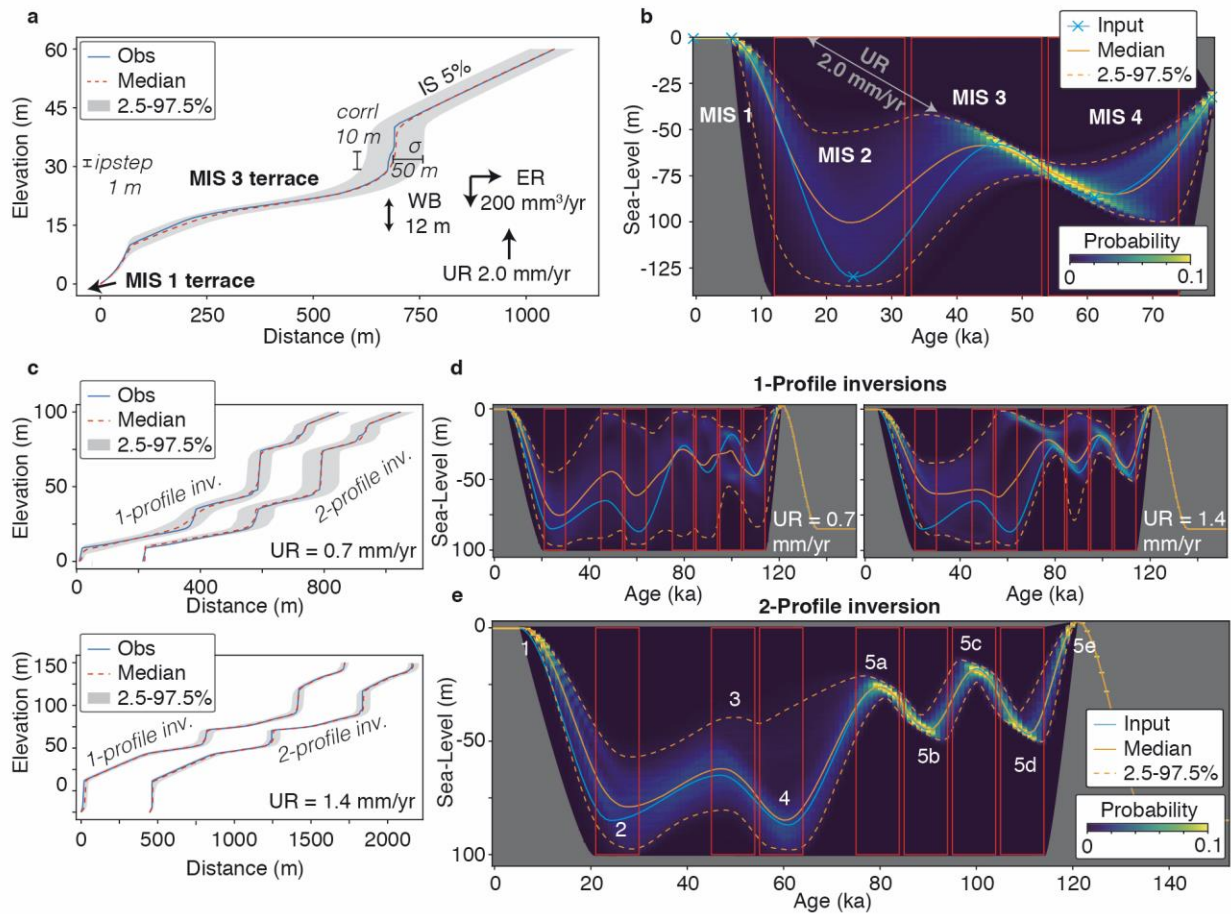
113
114 Then a residual power ($ER - dER_r/dt$) carves out a 1 m high notch and all its overhanging material to form a cliff.
115 Following previous studies (Anderson et al., 1999; Pastier et al., 2019), for K we use 0.1 as bedrock erodibility and 1
116 for notch carving. Finally, the 2D model we use consists of a landmass with a seaward dipping linear initial slope (IS;
117 Fig. 2a), an initial erosion rate (ER ; Fig. 2a) that evolves as platforms are being carved, a wave base depth (WB ; Fig.
118 2a) that determines the vertical range over which erosion takes place, a land uplift rate (UR ; Fig. 2a) and a sea-level
119 history.

120 To invert the morphology of the marine terrace sequences, we parameterize sea-level history with a finite number of
121 unknown parameters. We use nodes interpolated through a cubic spline scheme (Fig. 2b; light blue). This creates sea-
122 level curves with similar characteristics to published sea-level curves (red line, Fig. 1c), in which the nodes represent
123 sea-level minima (lowstands) and maxima (highstands) that are typically linked to even and odd-numbered marine
124 isotope stages (MIS), respectively.

125 Reconstructing the sea-level history from present day observations of marine terrace sequences can be mathematically
126 formulated as a highly non-linear inverse problem where the solution is non-unique. To embrace this non-uniqueness,
127 the problem can be cast in a Bayesian (probabilistic) framework where the solution is a posterior probability
128 distribution describing the probability of the model parameters (here the past sea-level variations), given the observed
129 data (here the geometry of marine terraces). We use a Markov chain Monte Carlo algorithm to sample the posterior
130 distribution and explore the range of models that can explain the observed topography within errors. In the Monte
131 Carlo exploration of the model space, nodes can either be fixed at certain ages and elevations, or left free to move
132 within a prescribed range (e.g. red boxes in Fig. 2b,d,e). The 4 main erosion model parameters (IS, ER, WB, UR) can
133 also be fixed to chosen values, as done in the synthetic tests below, or left free within chosen ranges, as done for the
134 Santa Cruz and Corinth examples below. The algorithm samples the parameter space as a random walk, where at each
135 iteration a new sea level history model is proposed by perturbing the current one. The proposed model is then either
136 accepted or rejected following an acceptance rule based on the level of data fit of the current and proposed models.
137 The final solution is a large ensemble of paleo sea-level models that approximates the probabilistic solution. That is,
138 the distribution of models follows the posterior probability solution. Of the 1 million model runs per figure, the first
139 50 000 models were discarded as burn-in models. To verify that the random walk samples the target distribution, we
140 show a number of convergence diagnostics in Fig. S1, which includes parameter acceptance ratios and likelihood
141 evolution for all model runs in this article. For a review of Bayesian inference and Monte Carlo methods in the
142 geosciences, we refer the reader to Mosegaard and Sambridge (2002), and Gallagher et al. (2009).

143 One benefit of Bayesian inference is the ability to propagate uncertainty estimates from the observed measurements
144 towards the unknown model parameters. For that, a likelihood probability distribution needs to be defined, based on
145 a misfit function and on uncertainty estimates associated with observations. In this work, the data vector is defined as
146 a set of points measured on the shoreline with a vertical step size ($ipstep$; Fig. 2a). The misfit between this observed
147 topography and the modelled paleo-shoreline sequences is calculated on the horizontal axis. The elevation axis is
148 therefore divided in a regular grid, and the level of data fit is measured by comparing the horizontal distance between
149 observed and simulated horizontal position at each grid point. In this way, the terrace width is used as an observed
150 parameter. Uncertainties about the observed shorelines account for the inability of our numerical model to explain
151 observations, and can be due to both observational or modelling errors. These errors are supposed Gaussian and
152 described by a standard deviation (σ ; Fig. 2a) and the level of spatial correlation related to the spatial resolution of the
153 data ($corrl$; Fig 2a). In preliminary tests (Fig. S2) we also tested inversions with the misfit calculated along vertical
154 axes (i.e. comparing elevations between observed and estimated profiles), but found it harder to reproduce realistic
155 marine terrace sequences with a few m of terrace height variability, and a few hundred meter of terrace width
156 variability (e.g. Regard et al., 2017; De Gelder et al., 2020). We note that changing the misfit calculation from

157 horizontal to vertical misfit does not change the paleo sea-level posterior distribution (Fig. S2). The assigned ranges
 158 for input parameters are all treated as flat uniform priors, i.e. a prior distribution that assigns equal probability to all
 159 the values within the specified ranges.
 160



161
 162 **Figure 2. Inversion of synthetic marine terrace profiles.** **a)** Synthetic topography (Obs, blue) created from a forward model with
 163 known input parameters: IS = Initial Slope, ER = Erosion Rate, UR = Uplift Rate and WB = Wave Base. The posterior range of
 164 models that fit the observed topography with the given σ , $ipstep$ and $corrI$ (see text) is represented by the median (orange), and the
 165 2.5 and 97.5 percentiles of the inverted models (grey envelope). **b)** Posterior probability distribution for the sea-level histories.
 166 Each individual paleo sea-level history is described with 6 sea-level nodes linked with a cubic spline interpolation, of which the
 167 nodes at 78, 6 and 0 ka are fixed in time and elevation, and the other three nodes can move within the three red boxes. The input
 168 (target) sea-level history is given in light blue, and the probabilistic solution is depicted by the median (solid orange line) and the
 169 2.5 and 97.5 percentiles (dashed orange lines). **c)** Same as **a**, but with different uplift rates and sea-level histories. **d)** Sea-level
 170 histories for the inverted profiles in **c**, similar to **b** but with a different input sea-level history including more nodes. **e)** Similar to
 171 **d**, but inverting the two profiles simultaneously to find a common sea-level curve explaining both profiles. MIS are marked in
 172 white.

173 **3 Synthetic marine terrace profiles**

174 To test and illustrate the potential of the inversion approach, we inverted synthetic topographic profiles that were
 175 produced by forward models with known input parameters (Fig. 2). To start with a relatively short and simple sea-
 176 level range, we defined an 80 ka sea-level history consisting of 6 nodes (Fig. 2b; light blue). For the inversion, we
 177 fixed the nodes at 78, 6 and 0 ka, and the positions of the other three nodes were left as unknown model parameters
 178 to be recovered. In the Monte Carlo exploration of the model space, these three nodes were left free to move within a

179 prescribed range (red boxes in Fig. 2b). All other erosion model parameters (IS, ER, WB, UR; Fig. 2a) were fixed
180 during the inversion at the values used to produce the observed topographic profile. The parameters σ , *ipstep* and *corr1*
181 were set at 50, 1 and 10 m, respectively. We inverted the topographic profile between 0 and 60 m elevation by sampling
182 the parameter space with 1 million forward simulations. The solution is a large ensemble of sea-level histories that
183 reflect the probability of the paleo sea-level, given the synthetic coastline topography.

184 The resulting profiles show an MIS 3 terrace at an elevation range of ~15-30 m (Fig. 2a), whereas an MIS 1 terrace
185 lies below the present-day sea level, and is thus not considered in the inversion. As such, the range of sea-level histories
186 that could have created the MIS 3 terrace is narrower than for the MIS 1 terrace (Fig. 2b). This range is particularly
187 limited for the period of sea-level rise leading up to the MIS 3 peak, suggesting that uplifted marine terraces are more
188 likely to form during periods of relative sea-level rise. This is theoretically expected, as erosion scales with the total
189 duration of sea-level occupation (Malatesta et al., 2021), and simultaneous sea-level rise and land uplift implies
190 favorable conditions for the formation of marine terraces. Another notable feature is the distribution of possible sea-
191 level histories along a diagonal line that corresponds to the uplift rate. This line would reach the maximum terrace
192 elevation when extrapolated to $t=0$ ka, in line with classic graphical methods (Bloom and Yonekura, 1990). Although
193 the MIS 1 terrace is not inverted, there are some limitations to the magnitude and rate of sea-level rise between MIS
194 2 and MIS 1 (Fig. 2b), probably because this period determines how much of the MIS 3 terrace is eroded at its distal
195 edge.

196 For the inversion of every individual profile there should be a trade-off between younger, higher sea-level peaks and
197 older, lower sea-level peaks in line with the fixed uplift rate (as in Fig. 2b). These trade-off effects can be overcome
198 through the joint inversion of multiple profiles with different uplift rates, reducing the uncertainty in sea-level
199 reconstructions. To show this, we also inverted two different topographic profiles produced with different fixed uplift
200 rates but with the same sea-level history over a 135 ka timescale (the last glacial-interglacial cycle; Fig. 2c-e). When
201 the two profiles are inverted individually, the range of possible sea-level histories is relatively wide, and again the sea-
202 level peaks would follow a diagonal line parallel to the uplift rate (Fig. 2c, d). However, if we jointly invert both
203 profiles, i.e. assuming that a unique sea-level history would have created both marine terrace staircase morphologies,
204 the probability distribution for past sea-level narrows, and the median sea-level of the inversion better approximates
205 the input curve (Fig. 2e). The range is particularly narrow for the transgressions leading up to the MIS 5a and 5c
206 highstands, for which the corresponding terraces are well developed in the topographic profiles (Fig. 2c). Similar to
207 the MIS 1 terrace in Fig. 2a, the MIS 1 and 3 terraces in Fig. 2c would be located below sea level for the given
208 parameters, and thus the possible sea-level range is wider for the transgressions leading up to MIS 1 and 3 (Fig. 2d).
209 Also for these highstands though, the sea-level is better constrained for the joint inversion (Fig. 2e) than with the
210 individual inversions (Fig. 2d). This suggests that jointly inverting more profiles would increase even further our
211 ability to constrain sea-level histories. To understand what happens in scenarios in which more parameters are
212 unknown, we repeated the same tests (from Figures 2b-d) with broad prior ranges for the uplift rate, initial slope,
213 erosion rate and wave base height (Fig. S3). Also in this case the joint inversion provides much narrower posterior
214 ranges for paleo sea-level compared to the two individual profile inversions, and not too different from the cases with
215 fixed model parameters (Figs. 2b-d). The posterior ranges for all parameters are consistently smaller for the joint
216 inversions, compared to the individual inversions (Fig. S3).

217 These synthetic tests imply that in natural examples, sea-level reconstruction should also benefit from the inversion
218 of multiple marine terrace profiles if conditions change between those profiles. In this example we used two different
219 uplift rates for the joint inversion, which lead to a range in different terrace sequence morphologies (Fig. 2c), but an
220 approach where all parameters, including wave base, erosion rate or initial slope, are undefined a priori (or only within
221 a given range), should lead to a more realistic range of possible sea-level histories.

222 To put this method to the test in real cases, we selected two well-documented yet contrasting cases, Santa Cruz and
223 the Gulf of Corinth, each having their peculiarities that make them ideal to study the inversion of marine terraces.
224 Santa Cruz is well documented and possible parametric windows are quite narrow, making it an ideal benchmark site
225 for our method. On the other hand, the staircase sequence in the Gulf of Corinth, while equally well documented, is
226 particularly relevant to take advantage of the predictive capacities of our method. There, we can decipher the complex

227 interplay between vertical land motion and sea-/lake-level fluctuations in a semi-closed basin, and better reconstruct
228 its hydrodynamic history where paleoclimatic data are insufficient.

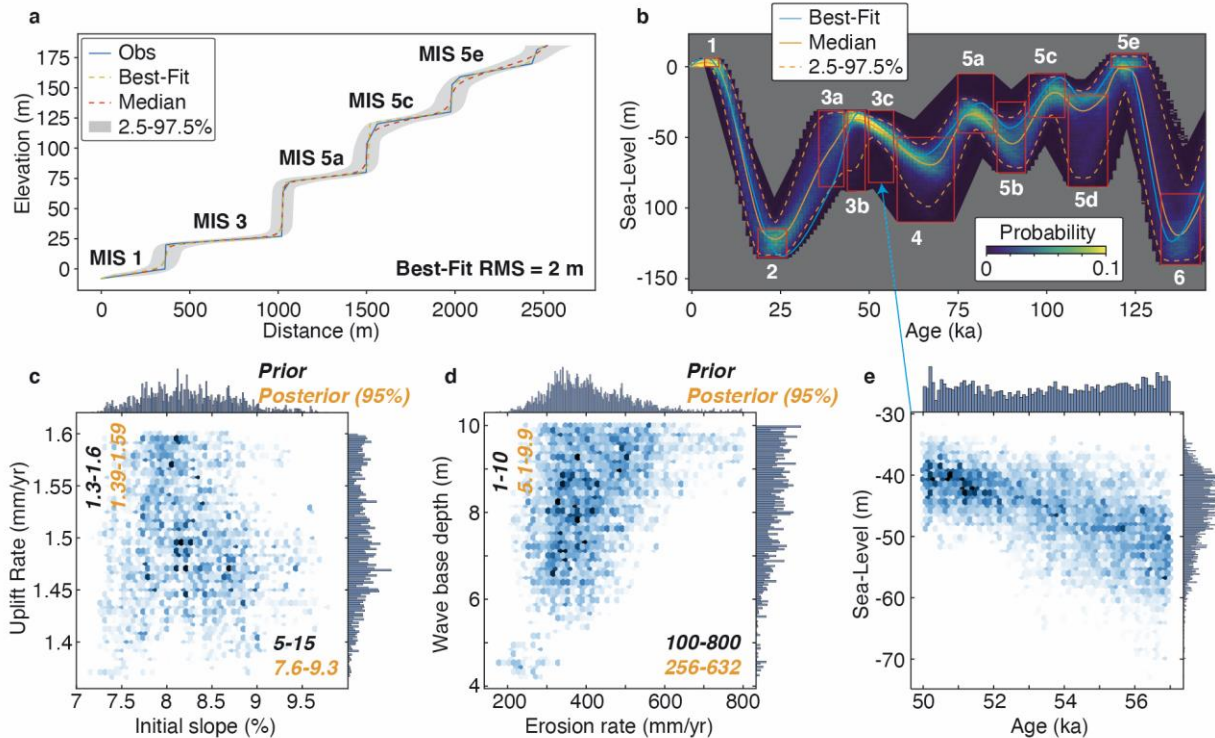
229 **4 Santa Cruz marine terrace sequence inversion**

230 The marine terraces along the Santa Cruz coastline (central California, US) formed through a combination of
231 Quaternary sea-level oscillations and tectonic uplift by nearby active faults (e.g. Bradley, 1957; Anderson and
232 Menking, 1994; Anderson et al., 1999; Perg et al., 2001; Matsumoto et al., 2022). We invert a topographic profile
233 from Rosenbloom and Anderson (1994), who distinguished the original eroded bedrock surface, which we use, from
234 its overlying colluvium for 5 marine terraces. We followed the age interpretation of Perg et al. (2001), suggesting
235 these terraces were formed, from bottom to top, during MIS 1, 3, 5a, 5c and 5e. Unlike in the synthetic tests, here we
236 left uplift rate, erosion rate, wave base depth and initial slope parameters free within a prior range of values. We use
237 the elevation (~170 m) and age (~118-128 ka) of the upper terrace to derive a range of possible uplift rates (1.3-1.65
238 mm/yr), and simultaneously consider ranges for initial slope (5-15%), wave base depth (1-10 m) and erosion rates
239 (100-800 mm³/yr) in the terrace inversion. We use the same inversion parameters as for the synthetic tests, running 1
240 million models over 450 ka with the sea-level high- and lowstands limited to the red boxes in Fig. 1 (See
241 Supplementary Information and Table S1). We tested different inversion parameters (Fig. S4), and settled on values
242 of 1 m *ipstep*, 100 m σ and 10 m *corrl*, as for these values the corresponding 95% posterior ranges for the variability
243 in terrace height (~5 m; Fig. S4) and width (~150 m; Fig. S4), are along the same order of magnitude as the variability
244 in a swath profile across the Santa Cruz terraces (Fig. S5). Higher values for σ and *corrl* result in both broader ranges
245 for accepted terrace heights/widths, and consequently also in broader posterior ranges for paleo sea-level, although
246 we note that the first order shape of the paleo sea-level curves remains similar irrespective of the tested *ipstep*, σ and
247 *corrl* values (Fig. S4).

248 The sampled sea-level histories successfully reproduce the terrace morphology, as evidenced by the low misfit of 2 m
249 (Fig. 3a). As with the synthetic tests (Fig. 2), periods of sea-level rise are better constrained than periods of sea-level
250 fall, and highstands better constrained than lowstands (Fig. 3b). Also here there is a trade-off in sea-level peaks, in
251 which younger, higher sea-level peaks could result in similar shaped marine terraces as older, lower sea-level peaks
252 (e.g. for MIS 3c, Fig. 3e). The models limit the uplift rate to ~1.35-1.6 mm/yr, the initial slope to ~7-9.5%, the wave
253 base depth to 4-10 m and the erosion rate to 200-800 mm/yr (Figs. 3c,d). Notably there is a positive correlation between
254 wave base depth and erosion rate (Fig. 3d), suggesting a higher value for wave base depth would require a higher
255 erosion rate to create the same marine terrace sequence morphology.

256 Compared to our proposed prior range of possible sea-level elevations for MIS 3 (-30 to -80 m; Fig. 3b), the posterior
257 distribution of the inversion suggests paleo sea-level values on the higher end of that spectrum. This is in agreement
258 with a growing number of studies suggesting oxygen-isotope derived sea-level curves underestimate sea-level for that
259 period (Pico et al., 2016; Dalton et al., 2019, 2022; Gowan et al., 2021; De Gelder et al., 2022). For MIS 5a on the
260 other hand, the posterior distribution of the inversion suggests a sea-level peak on the lower end of our proposed range
261 of sea-level elevations (Fig. 3b). Although the highstand posterior distributions still span a broad elevation range of
262 ~25 m, these results tend to align with studies proposing an overall decrease in sea-level between MIS 5e, 5c and 5a
263 (e.g. Chappell and Shackleton, 1986; Schellmann and Radtke, 2004; Tawil-Morsink et al., 2022).

264 We also tested additional uplift rate scenarios (Fig. S6), given that there has been concerns on the terrace chronology
265 that we adopted (Brown and Bourlès, 2002), and other studies have suggested the terrace at 27 m elevation might be
266 formed during MIS 5a, 5c or 5e instead of MIS 3 (Bradley and Addicott, 1968; Lajoie et al., 1975; Kennedy et al.,
267 1982; Weber et al., 1990). These uplift rates can fit the terrace sequence morphology equally well in terms of
268 topographic misfit, but generally imply a larger possible range of paleo sea level. This can be explained by the
269 increased terrace re-occupation for lower uplift rates (Malatesta et al., 2021), which also explains why the posterior
270 ranges for the initial slope and wave base depth change increase for lower uplift rate scenarios (Fig. S6), and erosion
271 rate estimates decrease. These tests suggest that locations with higher uplift rates will generally provide narrower
272 constraints on paleo sea-level, while still providing realistic and unbiased parameter estimates.



273
 274 **Figure 3. Inversion of NW-Santa Cruz marine terrace sequence.** a) Observed topography (from Rosenbloom and Anderson,
 275 1994; Obs, blue) with the age interpretation of Perg et al. (2001) marked in bold, together with the modeled best-fit, median, 2.5%
 276 and 97.5% percentile profiles. b) Probabilistic sea-level reconstruction for the profiles in a, MIS in white c) Posterior ranges for
 277 uplift rates and initial slopes (histogram of the sampled models), d) Posterior ranges for wave base depths and erosion rates e)
 278 Posterior ranges for the MIS 3c peak, i.e. distribution for the position of the 50-57 ka node within the paleo sea level curve.

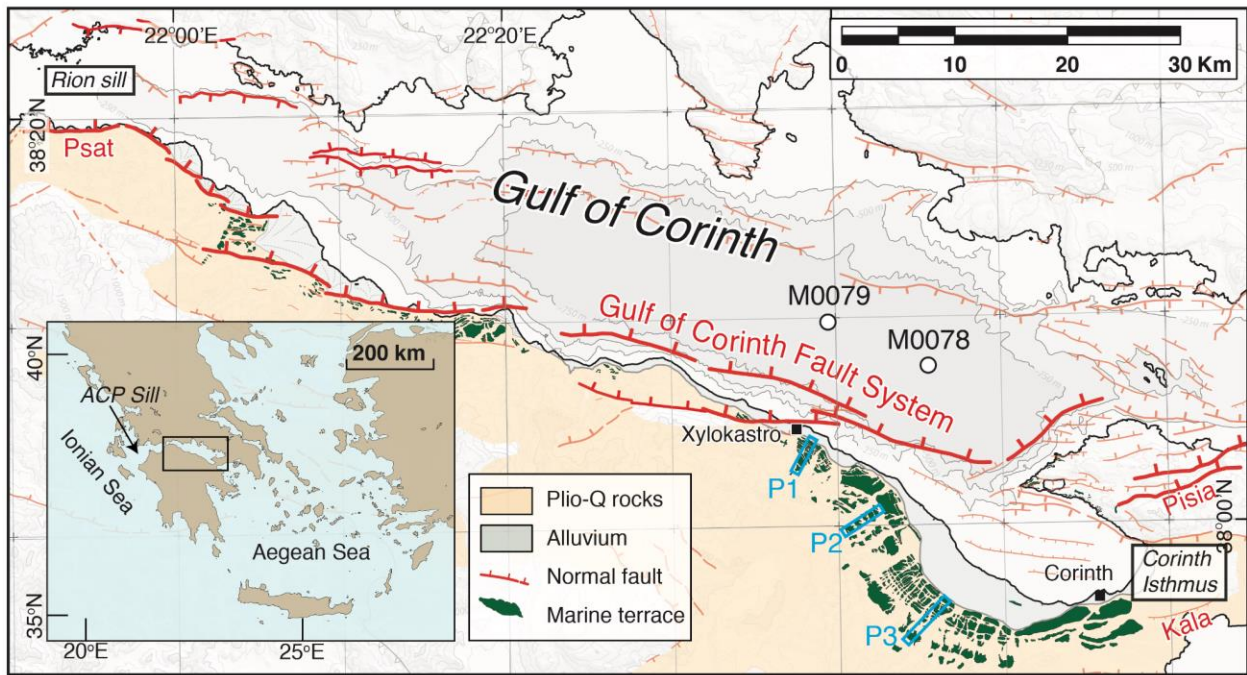
279 **5 Gulf of Corinth marine terrace sequence inversion**

280 The complexity of semi-isolated basins, connected to sea during some time intervals and isolated in others, make them
 281 ultimate testing grounds for our modelling approach. We focus on one of such basins, the SE Gulf of Corinth, to derive
 282 a sea-/lake-level history from terrace sequence geometries, and compare its outcomes to paleoclimate data, tectonic
 283 structures and sill dynamics.

284 Natural interaction between the Gulf of Corinth and the open sea is currently restricted by the Rion and Acheloo-
 285 Cape Pappas sills at its W entrance at ~45-60 m depth (Fig. 4; Beckers et al., 2016). In the past there was an additional
 286 connection at its E end along the Corinth Isthmus, currently uplifted at ~80 m elevation but consisting of Quaternary
 287 marine sediments (Fig. 4; Caterina et al., 2023). These sills have controlled the Gulf's connection with the open sea
 288 over the past few hundred thousand years and lead to an alternation of marine and (semi-)isolated lake environments
 289 within the Gulf (McNeill et al., 2019). Although we approximately know the timing of these alternations, it remains
 290 unclear whether sill depths remained stable or fluctuated throughout the Quaternary (Roberts et al., 2009; McNeill et
 291 al., 2019), and in addition, whether lake levels were stable or fluctuating during periods with no connection to the sea.
 292 Hydroclimatic conditions, i.e. the balance between inflow, outflow, precipitation and evaporation, determine the level
 293 of the lake, and state-of-the-art paleo-environmental reconstructions (e.g. Kafetzidou et al., 2023) are insufficient to
 294 infer its fluctuations over time.

295 Terrace sequences are well exposed in the SE of the Gulf, where the Gulf of Corinth Fault System (Fig. 4) has lead to
 296 differential coastal uplift rates (Armijo et al., 1996; De Gelder et al., 2019; Fernández-Blanco et al., 2019; Fig. S7).
 297 This peculiarity allows us to test on a natural example whether the joint inversion of multiple terrace sequence profiles
 298 with different uplift rates provides a better-constrained sea-/lake-level history (as in Fig. 2). To account for the

299 unknown range of possible lake-level elevations, we carried out inversions with all nodes from (semi-)isolated periods
 300 broadly constrained between -15 and -150 m elevation. We selected three topographic profiles with little river incision
 301 and ~0.4-1.4 mm/yr uplift rates (Fig. S7), and avoided modelling the broad coastal plains at the base of all profiles
 302 that appear to have been modified by human presence (Fig. S7). We used the 90% percentile of 100-m wide swath
 303 profiles to obtain representative terrace sequence morphologies (Fig. S7). For the three profiles we assigned prior
 304 ranges of possible uplift rates of 1.25-1.4, 0.7-0.9 and 0.4-0.55 mm/yr (De Gelder et al., 2019; Fig. S6), and broad
 305 prior ranges for erosion rate (100-1500 mm/yr), initial slope (1-20%) and wave base depth (1-12 m).
 306

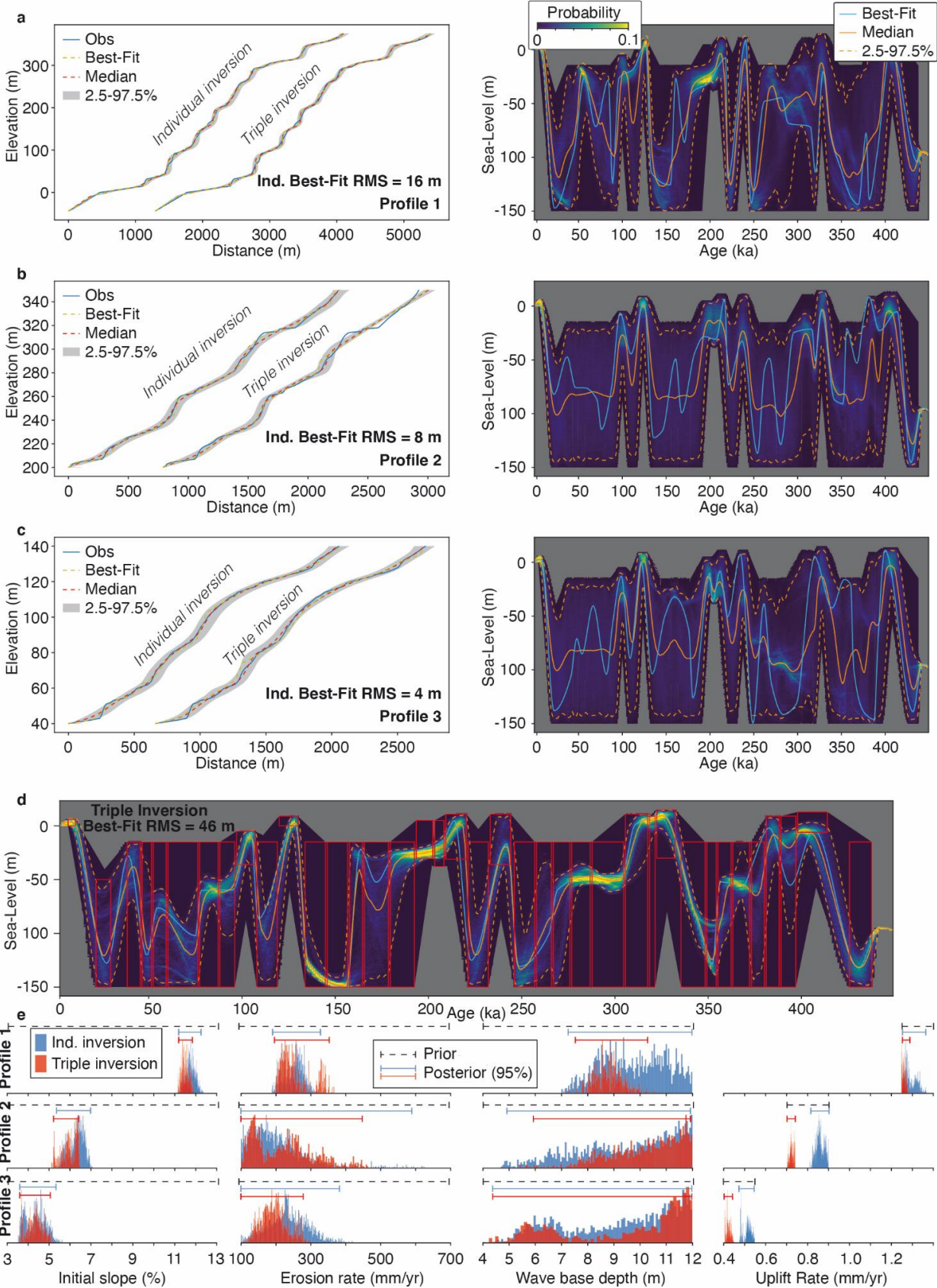


307
 308 **Figure 4. Tectonomorphology of the Gulf of Corinth.** Map showing the main features of the Gulf of Corinth, including the active
 309 faults, marine terraces, profile locations used in the inversion and connections to the Ionian Sea (Rion Sill) and Aegean Sea (Corinth
 310 Isthmus). M0078 and M0079 indicate the IODP-381 sedimentary coring locations (McNeill et al., 2019). Psat = Psathopyrgos
 311 Fault, Pisia = Pisia Fault, Kála = Kalamaki Fault. Modified from de Gelder et al. (2019) and Fernández-Blanco et al. (2020).

312 The individual profile inversions mostly constrain paleo sea/lake level for profile 1 (Fig. 5a), because it has the highest
 313 uplift rate and contains most terraces. The other two profiles provide limited constraints on paleo sea/lake level when
 314 inverted individually (Fig. 5b/c), but when jointly inverted with profile 1 they provide a much narrower range in terms
 315 of posterior distribution for sea-level (Fig. 5d). The cumulative misfit for the individual inversions (28 m) is slightly
 316 better than for the joint inversion (46 m), but there are no major visible differences between the terrace sequence
 317 profiles for the two inversions, and apart from the highest terrace of profile 2 (Fig. 5b) the terrace sequences are all
 318 near perfectly reconstructed. The three profiles show variations in initial slopes that are in line with the overall
 319 morphology, i.e. present-day profile 1 is steeper than 2, which is steeper than 3, which is also what we find for their
 320 initial slopes. The three profiles do have similar posterior distributions for wave base depths and erosion rates (Fig.
 321 5e). Although we might expect lateral differences in these rates given variability in sediment types, catchment area
 322 and coastal orientation, the broad ranges for the posterior distributions indicate we cannot quantify these lateral
 323 differences from the profile morphology alone. The posterior parameter ranges mostly remain the same between the
 324 individual and joint inversion, with exception of the uplift rates for profiles 2 and 3 that became a little lower for the
 325 joint inversion. As for the sea-/lake-level inversion, all the other posterior parameter ranges become narrower for the
 326 joint inversion (Fig. 5e).

327 The inverted sea-/lake-level history (Fig. 5d) shows a few notable features. To a first order, fluctuations resemble
 328 global sea-level trends, with relatively fast periods of sea-/lake-level rise prior to major sea-level highstands, followed

329 by long periods of slow sea-/lake-level fall (Fig. 1c). Yet, unlike global sea-level trends, there are several periods of
330 prolonged stability, in particular around 180-200 ka and 275-300 ka, and possibly also around 75-95 ka and 360-370
331 ka. In addition, glacial periods are often surprisingly poorly resolved, like during the period 20-75 ka or 160-180 ka.
332 In the last section we discuss our interpretation of these trends, and show how they provide insightful arguments to
333 decipher the relation between water level, fault activity, paleoclimate and tectonics.



335 **Figure 5. Inversion of SE Corinth Rift marine terrace sequence.** a-c) Observed topography (left) from 3 different profiles in
336 the SE Corinth Rift (locations see Fig. S7), together with the modeled best-fit, median, 2.5% and 97.5% percentile profiles for both
337 an individual profile inversion and a joint inversion of the three profiles (horizontally offset by an arbitrary value). Corresponding
338 probabilistic sea/lake-level ranges for the individually inverted profiles are given on the right, d) Posterior distribution for sea/lake-
339 level history from joint inversion, with red boxes describing prior ranges e) Prior and posterior parameter ranges from both
340 individual and joint profile inversions

341 **6 Discussion**

342 **6.1 Beyond sea level: tectono-hydro-climatic processes in the Gulf of Corinth**

343 While the results for the joint inversion of the 3 profiles in the Gulf of Corinth permit to unravel sea- and lake-levels
344 through time as expected, we also stress that such inversions yield more, when integrated within the broader
345 environmental setting: these reconstructions allow for a more detailed look into sea- and lake-level fluctuations within
346 a (semi-)isolated basin. Figure 6 compares our inverted sea-lake level to the stratigraphy, facies and pollen content
347 within two sedimentary cores from the sea floor of the central basin (McNeill et al., 2019; Gawthorpe et al., 2022;
348 Kafetzidou et al., 2023). Based on those combined datasets, we propose that the main hydroclimatic modes that have
349 occurred in the Gulf of Corinth throughout the past 450 ka, are 1) marine Gulf of Corinth, 2) transitional Gulf of
350 Corinth or overfilled Lake Corinth and 3) underfilled Lake Corinth. The first 2 of those have been proposed before
351 based on sedimentary cores (McNeill et al., 2019; Gawthorpe et al., 2022), whereas we base the occurrence of intervals
352 with an underfilled Lake Corinth on our marine/lake terrace inversion, as available paleoclimatic proxies are unable
353 to uncover them.

354 The major peaks in our reconstructed sea/lake-level curve occurred during interglacial sea-level highstands, when sea
355 level in the Gulf of Corinth was similar to eustatic sea level (marine mode M). Sedimentary cores indicate marine
356 conditions (McNeill et al., 2019), the corresponding stratal packages are bioturbated, and associated sedimentary
357 facies are types FA1 and FA6 (Fig. 6; see caption for facies description). From pollen records, the typical reconstructed
358 biomes are cool mixed evergreen needleleaf and deciduous broadleaf forests, indicating relatively warm and wet
359 conditions with low amounts of steppic taxa (Kafetzidou et al., 2023; Fig. 6).

360 We interpret the interstadial periods around 75-95 ka, 180-200 ka, 275-300 ka and 360-370 ka as periods with an
361 overfilled Lake Corinth, possibly with some marine incursions indicating a transitional Gulf of Corinth (T/O mode).
362 This would explain the prolonged sea-/lake-level stability, during interstadial periods when eustatic sea-level
363 fluctuated by tens of meters (e.g. Spratt and Lisiecki, 2016; De Gelder et al., 2022). In that case, sea-/lake-level
364 elevations would correspond to the paleo-sill depth of the Rion Sill and/or Corinth Isthmus (white line, Fig. 6). Within
365 the sedimentary cores, these periods are mostly characterized by laminated stratal packages, and associated
366 sedimentary facies are types FA2, FA3 and FA4 (Fig. 6; see caption for facies description). The occurrence of marine
367 incursions into Lake Corinth during these interstadial periods is suggested by dated corals of ~76 ka, ~178 ka and
368 ~201 ka (Roberts et al., 2009; Houghton et al., 2003) as well as the white, aragonite-rich laminations of FA3 and FA4.
369 In other locations such laminations have been linked to (seasonal) mixing of marine and non-marine surface waters
370 (Sondi and Juracic, 2010; Roeser et al., 2016).

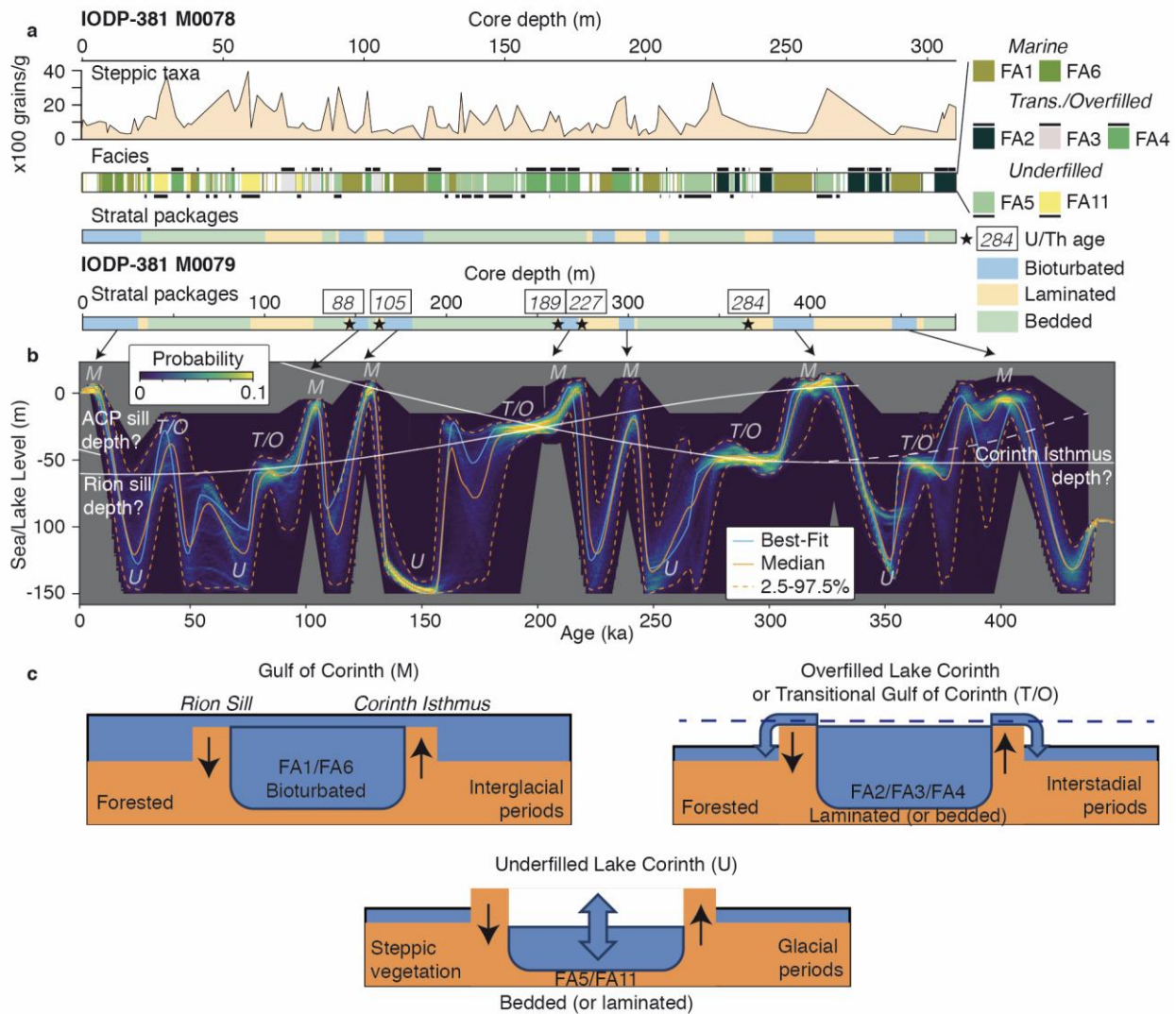
371 The glacial periods are characterized by relatively low sea/lake-level elevations, possibly even down to the lower limit
372 of -150 m we used in the inversion. We interpret these periods as underfilled Lake Corinth conditions (U mode),
373 during which water inflow was lower than water evaporation within the lake, and lake level fell down to tens of meters
374 below the sill depth. Sedimentary cores indicate non-marine conditions (McNeill et al., 2019), the corresponding
375 stratal packages are mostly bedded and associated sedimentary facies are types FA5 and FA11 (Fig. 6; see caption for
376 facies description). Reconstructed biomes from pollen suggest an increase in open vegetation such as grassland and
377 steppe communities under colder and drier conditions (Kafetzidou et al., 2023; Fig. 6), matching reconstructed periods
378 of lake underfilling. In general the inverted resolution of the lake-level elevation is much lower for these periods, with
379 large probabilistic ranges. We attribute this to the occurrence of rapid lake-level fluctuations, like in other isolated E-
380 Mediterranean water bodies such as the Dead Sea (Stein et al., 2010) and Lake Van (Turkey; Landmann et al., 1996).
381 In such environments, the lake level is determined by the budget between runoff and evaporation, and quick variations

382 are expected. Alternatively, this could also be due to the fact that terraces formed during low sea/lake level get
383 increasingly eroded during transgressions.

384 The interstadial periods with prolonged sea-/lake-level stability also allow for a possible reconstruction of sill depths
385 through time (white lines, Fig. 6). The westernmost sill, the Acheloos-Cape Pappas Sill (Fig. 4), is currently at a depth
386 of ~45-48 m. While there are no major faults there, we can't exclude slow subsidence or uplift at a few tenths of
387 mm/yr, cumulating to a few tens of meters on the 100 kyr time scale. The Rion Sill, at the western entrance to the Gulf
388 of Corinth, is currently at ~62 m depth (Perissoratis et al., 2000). As it is located in the hanging wall of the
389 Psathopyrgos Fault (Fig. 5), active since at least the past ~200 ka (Houghton et al., 2003), the Rion Sill was unlikely
390 deeper in the past. We reconstruct the Rion Sill depth assuming marine incursions around ~76 ka (Roberts et al., 2009)
391 took place through this sill, and the Rion Sill was not lower than sea/lake level during the overfilled/transitional
392 interval around ~200 ka. Extrapolating the trend, it would make sense for the older connections between Lake/Gulf of
393 Corinth and the open sea to have occurred primarily through the Corinth Isthmus at the eastern end of the Gulf of
394 Corinth.

395 The Corinth Isthmus is currently at an elevation of ~80 m, and has been uplifted through the Pisia Fault, Kalamaki
396 Fault and/or a regional uplift (Armijo et al., 1996; Roberts et al., 2009; Caterina et al., 2022). We reconstruct the
397 Corinth Isthmus depth assuming lake/sea level during overfilled/transitional intervals around ~290 and ~360 ka
398 correspond to the Corinth Isthmus depth, and the isthmus was not lower than sea/lake level during the
399 overfilled/transitional interval around ~200 ka. Extrapolating this trend fits with the current Corinth Isthmus elevation
400 of ~80 m. The isthmus elevation before ~360 ka is difficult to constrain from our data, but was possibly shallower
401 before, given the small amount of marine sediments deposited around the ~400 ka interglacial period, and the lack of
402 deposits within the Isthmus stratigraphy older than ~350 ka (Collier and Dart, 1991; Caterina et al., 2022). Our
403 reconstruction of both Rion Sill and Corinth Isthmus fits with the sedimentary interpretation of a tidal strait around
404 ~300 ka at the isthmus, with marine connections on both ends of the Gulf of Corinth (Caterina et al., 2022).

405 Our exploration of sea-/lake-level variations in the Gulf of Corinth demonstrates the strength of using marine terrace
406 sequence inversion. Although several questions remain – like the effects of erosion and sedimentation on sill evolution,
407 or the effects of non-constant uplift rates of the marine terrace sequences – we are able to provide a solid framework
408 that can explain several different tectonic and hydro-climatic processes simultaneously. We distinguish 4 different
409 hydroclimatic modes for the Lake/Gulf of Corinth, that have probably also occurred in other (semi-)isolated basins
410 like the Sea of Marmara or the Carioco Basin. Marine and transitional modes will most likely depend on eustatic sea-
411 level elevations and sill depths, whereas over- or underfilled lakes likely depend on sill depths and local climatic
412 conditions. For the Corinth Lake we show that this transition from over- to underfilled lakes occurs during changes
413 from interstadial to glacial periods, and is accompanied by changes in vegetation that imply drier conditions.



415
 416 **Figure 6. Comparison of sea-/lake-level reconstruction to other datasets.** a) Comparison to IODP-381 cores M0078 and M0079,
 417 with steppic taxa from Kafetzidou et al. (2023), facies from McNeill et al. (2019) and stratal packages with U/Th ages from
 418 Gawthorpe et al. (2022). FA1: homogenous mud, FA2: greenish gray mud with dark gray to black silty-to-sandy beds (cm-scale),
 419 FA3: light gray to white sub-mm laminations (cc or aragonite) alternating with mud-silt beds, FA4: laminated greenish gray to
 420 gray mud with muddy beds, FA5: greenish gray mud with homogeneous cm thick gray mud beds, FA6: green bedded partly
 421 bioturbated mud, silt and sand, FA11: interbedded mud/silt and cm thick sand beds. b) Inversion result from Fig. 5d with proposed
 422 sill/isthmus elevations, marking periods with marine (M), transitional or overfilled (T/O) and underfilled (U) hydroclimatic modes.
 423 c) Schematic illustrations of the different hydroclimatic modes in the Lake/Gulf of Corinth.

424 6.2 Inversion of marine terrace sequences

425 In the examples above, we showed how to assess paleo sea-level variations, and simultaneously extract quantified
 426 metrics for morphotectonics and hydrodynamics, from the geometry of marine terrace sequences. Using a probabilistic
 427 inversion methodology set in a Bayesian framework, we avoid the simplifications of bijective approaches in which a
 428 single marine terrace is always linked to a single sea-level highstand and vice-versa (e.g. Pastier et al., 2019; Malatesta
 429 et al., 2021). By considering a full sea-level curve and its possible variability, it is possible to provide quantitative
 430 constraints on highstands, lowstands, sea-level rise and fall, filling the observational gap for time periods for which
 431 field measurements are scarce. We admit that some model simplifications and approximations may alter our

432 interpretations. In particular, we neglect subaerial erosion, and kept uplift rate, erosion rate, initial slope and wave
433 base depth parameters time-constant for each individual sampled paleo sea level curve. Both could be fine-tuned in
434 future developments.

435 To apply this model procedure to other sites, we can make several recommendations based on our findings in this
436 paper. Any coastal area with marine terraces will have lateral variability in terms of terrace width and terrace elevation.
437 Given that the posterior ranges for the model parameters (paleo sea-level, uplift rate, etc.) will directly depend on the
438 chosen inversion parameters (*ipstep*, σ and *corr1*), it is important to adjust those inversion parameters to the naturally
439 observed variability in the geometry of a marine terrace sequence. In the Santa Cruz example the similarity in terrace
440 width/height variability between the modeled posterior ranges (Fig. S4), and the observed variability within a section
441 of the marine terrace sequence (Fig. S5) justifies our choice of inversion parameters. But, if we wanted to characterize
442 a larger area along the Santa Cruz coastline, we would either have to increase σ and/or *corr1* to account for the higher
443 degree of variability, or jointly invert multiple cross-sections in which every cross-section has a similar variability in
444 terrace height/width.

445 The prior information required to obtain reliable results, will also be dependent on the context of a specific marine
446 terrace sequence, and on the parameter cut-off choices deemed realistic. For Santa Cruz and Corinth, the posterior
447 distributions for wave base depth suggest that, purely based on marine terrace sequence morphology, this cut-off could
448 have been deeper than 10-12 m (Figs. 3 and 5). However, based on observations and models of cliff erosion it seems
449 unlikely that the wave base for bedrock erosion is more than 10 m for Santa Cruz (Kline et al., 2014), and wave base
450 depths/heights should be smaller for the calmer Gulf of Corinth. This choice in cut-off in turn affects the posterior
451 distribution of other parameters, and should thus be chosen carefully.

452 In the cases of Corinth and Santa Cruz we assigned relatively narrow windows for the uplift rate, based on
453 chronological information that was already available. As such we only obtained refinements, rather than ‘new’
454 information about the uplift rate. For the Santa Cruz case, we tested four uplift rate scenarios matching different
455 possible chrono-stratigraphies (Fig. S6) that could all explain the morphology equally well, albeit with different ranges
456 for the other parameters. We also inverted the Santa Cruz terrace sequence morphology with a broad range between
457 0.3 and 1.5 mm/yr, but the inversion would converge on only one of the four scenarios in Fig. S6. This suggests that
458 at least an approximate prior idea on the uplift rate is a prerequisite for a reliable inversion of a marine terrace sequence
459 morphology.

460 Many paleo sea-level studies that use geomorphic/geologic observations tend to have a confirmation bias regarding
461 sea-level curves, and propose refinements of paleo sea-level estimates to sub-m scale (e.g. Murray-Wallace, 2002;
462 Roberts et al., 2012) or uplift rates to precisions of ~ 0.01 mm/yr (e.g. Pedoja et al., 2018; Meschis et al., 2022). In this
463 study, we take a step back by allowing more freedom to possible paleo sea-level variations, as well as uplift rate,
464 erosion rate, initial slope and wave base depth, to provide a more reliable way to translate morphologic observations
465 to paleo sea-level constraints. For instance, the low uplift rate examples from the Corinth Rift (Fig. 5b, c) and Santa
466 Cruz (Fig. S6) reveal very little about paleo sea/lake levels, even if the uplift rate is roughly known. As a marine
467 terrace is formed over several sea-level cycles, the resulting terrace width and height will depend on all those cycles,
468 as well as wave base depths, erosion rates and initial slopes, all of which are generally poorly constrained. Even in the
469 hypothetical case that these parameters are known (Fig. 2), there is still a wide spectrum of sea-level histories that
470 could have created the specific morphology of a marine terrace sequence. It suggests that estimating paleo sea-level
471 based on the comparison of a present-day landform to a paleo-landform (Rovere et al., 2016), may be too simplistic
472 in many cases, at least for erosive marine terraces. Although uncertainties that we provide on paleo sea-level are much
473 larger than what calculations based on hydrodynamic ranges would suggest (Lorchsteid and Rovere, 2019), we do
474 consider them to be reliable as they take in a large number of unknowns.

475 Although here we focused on erosive marine terraces to develop a proof of concept, a promising avenue is to apply
476 this inversion method to bio-constructed (coral reef) terraces, which tend to be better dated (e.g. Pedoja et al., 2014;
477 Hibbert et al., 2016) and for which modelling routines also exist (e.g. Toomey et al., 2013; Pastier et al., 2019). One
478 of our key findings is that inverting multiple profiles simultaneously provides much better paleo sea-level constraints
479 than focusing on individual profiles (Figs. 2, 5). The global archive of paleo-shorelines (Fig. 1a) presents a huge
480 potential for such multi-profile marine terrace inversions. This massive inversion would not only lead to improved

481 estimates of local relative sea-level histories, but may also complement studies on glacio-isostatic adjustments that
482 are relevant to a global sea-level perspective.

483 **7 Conclusions**

484 In this study we demonstrated the use of a probabilistic inversion approach to decipher the formation of marine terrace
485 sequences in general, and the tectonic and hydro-climatic evolution of (semi-)isolated basins in particular. With this
486 approach, we provide the tools (see below) to simultaneously estimate past sea-level variations, uplift rates, erosion
487 rates, initial slopes and wave heights.

488 From synthetic tests, benchmarking on a terrace sequence near Santa Cruz marine terrace sequence, and application
489 to the sequence in the SE Gulf of Corinth, our results bring a theoretical advance by showing that : 1) Paleo sea-level
490 and other parameter ranges can be better constrained from sequences that are uplifting at higher rates compared to
491 lower rates, and better constrained from a joint inversion of multiple profiles than from inversion of a single profile.
492 2) Uplift rates, sea-level variations and wave erosion parameters are intricately linked. By allowing more freedom to
493 possible ranges of all the relevant parameters, we provide a more reliable way to translate morphologic observations
494 to paleo sea-level constraints. Resulting uncertainties may be higher compared to ‘classic’ approaches of comparing
495 present to past shoreline elevations, but are more realistic. 3) Probabilistic inversion of marine terrace sequences is a
496 powerful method, applicable to a large portion of the world’s coastlines to disentangle tectonic and hydro-climatic
497 processes.

498 Beyond the methodological achievement, by applying our method to a complex case -the semi-isolated Gulf of Corinth
499 (Greece), we show that this method can be a powerful tool to explore subtle environmental forcings, like the balance
500 between precipitation and evaporation, that may have had a prime importance in setting the lake level during certain
501 periods of time. We found that eustatic sea-level and tectonically changing sill depths drive marine and transitional
502 phases during interglacial and interstadial periods, respectively. Wetter and drier conditions drive over- and
503 underfilling of Lake Corinth during interstadial and glacial periods, respectively. We expect such transitions to be
504 different for each unique tectono-hydro-climatic setting, with our inversion approach providing a new way to decipher
505 such geomorphic Rosetta stones.

506 **Code availability**

507 The marine terrace inversion code used in this study can be found at <https://github.com/ginodegelder/Rosetta>.

508 **Supplement link**

509 The supplementary material to this study can be found at <https://doi.org/10.31223/X5B117>.

510 **Author contribution**

511 **Conceptualization** by GdG, LH and TB, **Formal analysis** by GdG, **Funding acquisition** by TB, **Investigation** by
512 GdG, NH, LH and TB, **Methodology** by GdG, NH, AMP, TB and YB, **Visualization** by GdG, NH and YB, **Writing**
513 **- original draft** by GdG, **Writing - review & editing** by all authors.

514 **Competing interests**

515 The authors declare that they have no conflict of interest.

516

517 **Acknowledgements**

518 This study has been funded by the European Union horizon 2020 research and innovation program under grant
519 agreement 716542. Furthermore, GdG acknowledges postdoctoral funding from the IRD and the Manajemen Talenta
520 BRIN fellowship program, and research permit 52/SIP.EXT/IV/FR/5/2023 provided by the Indonesian government
521 on May 11th 2023 . GdG likes to thank Katerina Kouli for sharing her pollen data, and other IODP-381 expedition
522 members, as well as David Fernández-Blanco, Robin Lacassin and Rolando Armijo, for the many fruitful discussions
523 on the Corinth Rift.

524 **References**

- 525 Aksu, A. E., Hiscott, R. N., & Dogan, Y. (1999). Oscillating Quaternary water levels of the Marmara Sea and vigorous
526 outflow into the Aegean Sea from the Marmara Sea–Black Sea drainage corridor. *Marine Geology*, 153(1-4), 275-
527 302.
- 528 Andersen, M. B., Stirling, C. H., Potter, E. K., Halliday, A. N., Blake, S. G., McCulloch, M. T., ... & O’Leary, M. J.
529 (2010). The timing of sea-level high-stands during Marine Isotope Stages 7.5 and 9: Constraints from the uranium-
530 series dating of fossil corals from Henderson Island. *Geochimica et Cosmochimica Acta*, 74(12), 3598-3620.
- 531 Anderson, R.S., Densmore, A.L., Ellis, M.A., 1999. The generation and degradation of marine terraces. *Basin Res.* 11
532 (1), 7e19.
- 533 Anderson, R. S., & Menking, K. M. (1994). The Quaternary marine terraces of Santa Cruz, California: Evidence for
534 coseismic uplift on two faults. *Geological Society of America Bulletin*, 106(5), 649-664.
- 535 Armijo, R., Meyer, B. G. C. P., King, G. C. P., Rigo, A., & Papanastassiou, D. (1996). Quaternary evolution of the
536 Corinth Rift and its implications for the Late Cenozoic evolution of the Aegean. *Geophysical Journal International*,
537 126(1), 11-53.
- 538 Austermann, J., Mitrovica, J. X., Huybers, P., & Rovere, A. (2017). Detection of a dynamic topography signal in last
539 interglacial sea-level records. *Science Advances*, 3(7), e1700457.
- 540 Batchelor, C. L., Margold, M., Krapp, M., Murton, D. K., Dalton, A. S., Gibbard, P. L., ... & Manica, A. (2019). The
541 configuration of Northern Hemisphere ice sheets through the Quaternary. *Nature communications*, 10(1), 3713.
- 542 Beckers, A., Beck, C., Hubert-Ferrari, A., Tripsanas, E., Crouzet, C., Sakellariou, D., ... & De Batist, M. (2016).
543 Influence of bottom currents on the sedimentary processes at the western tip of the Gulf of Corinth, Greece. *Marine*
544 *Geology*, 378, 312-332.
- 545 Bernard, P., Lyon-Caen, H., Briole, P., Deschamps, A., Boudin, F., Makropoulos, K., ... & Linde, A. (2006).
546 Seismicity, deformation and seismic hazard in the western rift of Corinth: New insights from the Corinth Rift
547 Laboratory (CRL). *Tectonophysics*, 426(1-2), 7-30.
- 548 Bloom, A. L., & Yonekura, N. (1990). Graphic analysis of dislocated Quaternary shorelines. *Sea-level change*, 104-
549 115.
- 550 Bradley, W. C. (1957). Origin of marine-terrace deposits in the Santa Cruz area, California. *Geological Society of*
551 *America Bulletin*, 68(4), 421-444.
- 552 Bradley, W. C., & Addicott, W. O. (1968). Age of first marine terrace near Santa Cruz, California. *Geological Society*
553 *of America Bulletin*, 79(9), 1203-1210.
- 554 Brown, E. T., & Bourles, D. L. (2002). Use of a new ¹⁰Be and ²⁶Al inventory method to date marine terraces, Santa
555 Cruz, California, USA: Comment and Reply: COMMENT. *Geology*, 30(12), 1147-1148.
- 556 Caterina, B., Rubi, R., & Hubert-Ferrari, A. (2023). Stratigraphic architecture, sedimentology and structure of the
557 Middle Pleistocene Corinth Canal (Greece). *Geological Society, London, Special Publications*, 523(1), 279-304.
- 558 Chappell, J., & Shackleton, N. (1986). Oxygen isotopes and sea level. *Nature*, 324(6093), 137-140.
- 559 Chauveau, D., Pastier, A.-M., de Gelder, G., Husson, L., Authemayou, C., Pedoja, K. et al. (2024) Unravelling the
560 morphogenesis of coastal terraces at Cape Laundi (Sumba Island, Indonesia): Insights from numerical models. *Earth*
561 *Surface Processes and Landforms*, 49(2), 549–566.

562 Collier, R. L., & Dart, C. J. (1991). Neogene to Quaternary rifting, sedimentation and uplift in the Corinth Basin,
563 Greece. *Journal of the Geological Society*, 148(6), 1049-1065.

564 Collier, R. E., Leeder, M. R., Trout, M., Ferentinos, G., Lyberis, E., & Papatheodorou, G. (2000). High sediment
565 yields and cool, wet winters: Test of last glacial paleoclimates in the northern Mediterranean. *Geology*, 28(11), 999-
566 1002.

567 Creveling, J. R., Mitrovica, J. X., Clark, P. U., Waelbroeck, C., & Pico, T. (2017). Predicted bounds on peak global
568 mean sea level during marine isotope stages 5a and 5c. *Quaternary Science Reviews*, 163, 193-208.

569 Dalton, A. S., Finkelstein, S. A., Forman, S. L., Barnett, P. J., Pico, T., & Mitrovica, J. X. (2019). Was the Laurentide
570 Ice Sheet significantly reduced during marine isotope stage 3?. *Geology*, 47(2), 111-114.

571 Dalton, A. S., Pico, T., Gowan, E. J., Clague, J. J., Forman, S. L., McMartin, I., ... & Helmens, K. F. (2022). The
572 marine $\delta^{18}\text{O}$ record overestimates continental ice volume during Marine Isotope Stage 3. *Global and Planetary*
573 *Change*, 212, 103814.

574 De Gelder, G., Fernández-Blanco, D., Melnick, D., Duclaux, G., Bell, R. E., Jara-Muñoz, J., ... & Lacassin, R. (2019).
575 Lithospheric flexure and rheology determined by climate cycle markers in the Corinth Rift. *Scientific Reports*, 9(1),
576 4260.

577 De Gelder, G., Jara-Munoz, J., Melnick, D., Fernández-Blanco, D., Rouby, H., Pedoja, K., ... & Lacassin, R. (2020).
578 How do sea-level curves influence modeled marine terrace sequences?. *Quaternary Science Reviews*, 229, 106132.

579 De Gelder, G., Husson, L., Pastier, A. M., Fernández-Blanco, D., Pico, T., Chauveau, D., ... & Pedoja, K. (2022).
580 High interstadial sea levels over the past 420ka from the Huon Peninsula, Papua New Guinea. *Communications Earth*
581 *& Environment*, 3(1), 256.

582 De Gelder, G., Solihuddin, T., Utami, D. A., Hendrizan, M., Rachmayani, R., Chauveau, D., ... & Cahyarini, S. Y.
583 (2023). Geodynamic control on Pleistocene coral reef development: insights from northwest Sumba Island
584 (Indonesia). *Earth Surface Processes and Landforms*, 48(13), 2536-2553.

585 Derricourt, R. (2005). Getting “Out of Africa”: sea crossings, land crossings and culture in the hominin migrations.
586 *Journal of world prehistory*, 19, 119-132.

587 Dutton, A., Carlson, A. E., Long, A. J., Milne, G. A., Clark, P. U., DeConto, R., ... & Raymo, M. E. (2015). Sea-level
588 rise due to polar ice-sheet mass loss during past warm periods. *science*, 349(6244), aaa4019.

589 Dyer, B., Austermann, J., D’Andrea, W. J., Creel, R. C., Sandstrom, M. R., Cashman, M., ... & Raymo, M. E. (2021).
590 Sea-level trends across The Bahamas constrain peak last interglacial ice melt. *Proceedings of the National Academy*
591 *of Sciences*, 118(33), e2026839118.

592 Fernández-Blanco, D., de Gelder, G., Lacassin, R., & Armijo, R. (2019). A new crustal fault formed the modern
593 Corinth Rift. *Earth-Science Reviews*, 199, 102919.

594 Fernández-Blanco, D., de Gelder, G., Lacassin, R., & Armijo, R. (2020). Geometry of flexural uplift by continental
595 rifting in Corinth, Greece. *Tectonics*, 39(1), e2019TC005685.

596 Gallagher, K., Charvin, K., Nielsen, S., Sambridge, M., & Stephenson, J. (2009). Markov chain Monte Carlo (MCMC)
597 sampling methods to determine optimal models, model resolution and model choice for Earth Science problems.
598 *Marine and Petroleum Geology*, 26(4), 525-535.

599 Gallen, S. F., & Fernández-Blanco, D. (2021). A new data-driven Bayesian inversion of fluvial topography clarifies
600 the tectonic history of the corinth rift and reveals a channel steepness threshold. *Journal of Geophysical Research:*
601 *Earth Surface*, 126(3), e2020JF005651.

602 Gawthorpe, R. L., Fabregas, N., Pechlivanidou, S., Ford, M., Collier, R. E. L., Carter, G. D., ... & Shillington, D. J.
603 (2022). Late Quaternary mud-dominated, basin-floor sedimentation of the Gulf of Corinth, Greece: Implications for
604 deep-water depositional processes and controls on syn-rift sedimentation. *Basin Research*, 34(5), 1567-1600.

605 Gowan, E. J., Zhang, X., Khosravi, S., Rovere, A., Stocchi, P., Hughes, A. L., ... & Lohmann, G. (2021). A new global
606 ice sheet reconstruction for the past 80 000 years. *Nature communications*, 12(1), 1199.

607 Guilcher, A., 1974. Les «rasas»: un problème de morphologie littorale générale. *Annales de Géographie*, 83, 1–33.

608 Hay, C., Mitrovica, J. X., Gomez, N., Creveling, J. R., Austermann, J., & Kopp, R. E. (2014). The sea-level
609 fingerprints of ice-sheet collapse during interglacial periods. *Quaternary Science Reviews*, 87, 60-69.

610 Hibbert, F. D., Rohling, E. J., Dutton, A., Williams, F. H., Chutcharavan, P. M., Zhao, C., & Tamisiea, M. E. (2016).
611 Coral indicators of past sea-level change: A global repository of U-series dated benchmarks. *Quaternary Science*
612 *Reviews*, 145, 1-56.

613 Houghton, S. L., Roberts, G. P., Papanikolaou, I. D., McArthur, J. M., & Gilmour, M. A. (2003). New 234U-230Th
614 coral dates from the western Gulf of Corinth: Implications for extensional tectonics. *Geophysical Research Letters*,
615 30(19).

616 Husson, L., Pastier, A.-M., Pedoja, K., Elliot, M., Paillard, D., Authemayou, C., et al., 2018. Reef carbonate
617 productivity during quaternary sea level oscillations. *Geochem. Geophys. Geosyst.* 19 (4), 1148e1164.

618 Jara-Muñoz, J., Melnick, D., Pedoja, K., & Strecker, M. R. (2019). TerraceM-2: A Matlab® interface for mapping
619 and modeling marine and lacustrine terraces. *Frontiers in Earth Science*, 255.

620 Johnson, M. E., & Libbey, L. K. (1997). Global review of upper Pleistocene (substage 5e) rocky shores: tectonic
621 segregation, substrate variation, and biological diversity. *Journal of Coastal Research*, 297-307.

622 Kafetzidou, A., Fatourou, E., Panagiotopoulos, K., Marret, F., & Kouli, K. (2023). Vegetation Composition in a
623 Typical Mediterranean Setting (Gulf of Corinth, Greece) during Successive Quaternary Climatic Cycles. *Quaternary*,
624 6(2), 30.

625 Kennedy, G. L., Lajoie, K. R., & Wehmiller, J. F. (1982). Aminostratigraphy and faunal correlations of late Quaternary
626 marine terraces, Pacific Coast, USA. *Nature*, 299(5883), 545-547.

627 Kline, S. W., Adams, P. N., & Limber, P. W. (2014). The unsteady nature of sea cliff retreat due to mechanical
628 abrasion, failure and comminution feedbacks. *Geomorphology*, 219, 53-67.

629 Kopp, R. E., Simons, F. J., Mitrovica, J. X., Maloof, A. C., & Oppenheimer, M. (2009). Probabilistic assessment of
630 sea level during the last interglacial stage. *Nature*, 462(7275), 863-867.

631 Landmann, G., Reimer, A., & Kempe, S. (1996). Climatically induced lake level changes at Lake Van, Turkey, during
632 the Pleistocene/Holocene transition. *Global Biogeochemical Cycles*, 10(4), 797-808.

633 Lajoie, K. R., Wehmiller, J. F., Kvenvolden, K. A., Peterson, E., & White, R. H. (1975). Correlation of California
634 marine terraces by amino acid stereochemistry. In *Geological Society of America Abstracts with Programs* (Vol. 7,
635 No. 3, pp. 338-339).

636 Lajoie, K.R., 1986. Coastal tectonics. In: Press, N.A. (Ed.), *Active Tectonics*. National Academic Press, Washington
637 DC, pp. 95e124.

638 Lambeck, K., & Chappell, J. (2001). Sea level change through the last glacial cycle. *Science*, 292(5517), 679-686.

639 Leclerc, F., & Feuillet, N. (2019). Quaternary coral reef complexes as powerful markers of long-term subsidence
640 related to deep processes at subduction zones: Insights from Les Saintes (Guadeloupe, French West Indies).
641 *Geosphere*, 15(4), 983-1007.

642 Lorscheid, T., & Rovere, A. (2019). The indicative meaning calculator—quantification of paleo sea-level relationships
643 by using global wave and tide datasets. *Open Geospatial Data, Software and Standards*, 4, 1-8.

644 Malatesta, L. C., Finnegan, N. J., Huppert, K. L., & Carreño, E. I. (2022). The influence of rock uplift rate on the
645 formation and preservation of individual marine terraces during multiple sea-level stands. *Geology*, 50(1), 101-105.

646 Marra, F., Sevink, J., Tolomei, C., Vannoli, P., Florindo, F., Jicha, B. R., & La Rosa, M. (2023). New age constraints
647 on the MIS 9–MIS 5.3 marine terraces of the Pontine Plain (central Italy) and implications for global sea levels.
648 *Quaternary Science Reviews*, 300, 107866.

649 Matsumoto, H., Young, A. P., & Carilli, J. E. (2022). Modeling the relative influence of environmental controls on
650 marine terrace widths. *Geomorphology*, 396, 107986.

651 McNeill, L. C., Shillington, D. J., Carter, G. D., Everest, J. D., Gawthorpe, R. L., Miller, C., ... & Green, S. (2019).
652 High-resolution record reveals climate-driven environmental and sedimentary changes in an active rift. *Scientific*
653 *Reports*, 9(1), 3116.

654 Medina-Elizalde, M. (2013). A global compilation of coral sea-level benchmarks: implications and new challenges.
655 *Earth and Planetary Science Letters*, 362, 310-318.

656 Meschis, M., Roberts, G. P., Robertson, J., Mildon, Z. K., Sahy, D., Goswami, R., ... & Iezzi, F. (2022). Out of phase
657 Quaternary uplift-rate changes reveal normal fault interaction, implied by deformed marine palaeoshorelines.
658 *Geomorphology*, 416, 108432.

659 Mosegaard, K., & Sambridge, M. (2002). Monte Carlo analysis of inverse problems. *Inverse problems*, 18(3), R29.

660 Murray-Wallace, C. V. (2002). Pleistocene coastal stratigraphy, sea-level highstands and neotectonism of the southern
661 Australian passive continental margin—a review. *Journal of Quaternary Science: Published for the Quaternary
662 Research Association*, 17(5-6), 469-489.

663 Nixon, C. W., McNeill, L. C., Bull, J. M., Bell, R. E., Gawthorpe, R. L., Henstock, T. J., ... & Kranis, H. (2016). Rapid
664 spatiotemporal variations in rift structure during development of the Corinth Rift, central Greece. *Tectonics*, 35(5),
665 1225-1248.

666 Ott, R. F., Gallen, S. F., Wegmann, K. W., Biswas, R. H., Herman, F., & Willett, S. D. (2019). Pleistocene terrace
667 formation, Quaternary rock uplift rates and geodynamics of the Hellenic Subduction Zone revealed from dating of
668 paleoshorelines on Crete, Greece. *Earth and Planetary Science Letters*, 525, 115757.

669 Pastier, A.-M., Husson, L., Pedoja, K., Bezos, A., Authemayou, C., Arias-Ruiz, C., Cahyarini, S.Y. (2019). Genesis
670 and architecture of sequences of quaternary coral reef terraces: Insights from numerical models. *Geochem. Geophys.
671 Geosyst.*, 20 (8), 4248e4272.

672 Pedoja, K., Husson, L., Regard, V., Cobbold, P. R., Ostanciaux, E., Johnson, M. E., ... & Delcaillau, B. (2011).
673 Relative sea-level fall since the last interglacial stage: are coasts uplifting worldwide?. *Earth-Science Reviews*, 108(1-
674 2), 1-15.

675 Pedoja, K., Husson, L., Johnson, M. E., Melnick, D., Witt, C., Pochat, S., ... & Garestier, F. (2014). Coastal staircase
676 sequences reflecting sea-level oscillations and tectonic uplift during the Quaternary and Neogene. *Earth-Science
677 Reviews*, 132, 13-38.

678 Pedoja, K., Jara-Muñoz, J., De Gelder, G., Robertson, J., Meschis, M., Fernández-Blanco, D., ... & Pinel, B. (2018).
679 Neogene-Quaternary slow coastal uplift of Western Europe through the perspective of sequences of strandlines from
680 the Cotentin Peninsula (Normandy, France). *Geomorphology*, 303, 338-356.

681 Perg, L. A., Anderson, R. S., & Finkel, R. C. (2001). Use of a new ¹⁰Be and ²⁶Al inventory method to date marine
682 terraces, Santa Cruz, California, USA. *Geology*, 29(10), 879-882.

683 Perissoratis, C., Piper, D. J. W., & Lykousis, V. (2000). Alternating marine and lacustrine sedimentation during late
684 Quaternary in the Gulf of Corinth rift basin, central Greece. *Marine Geology*, 167(3-4), 391-411.

685 Pico, T., Mitrovica, J. X., Ferrier, K. L., & Braun, J. (2016). Global ice volume during MIS 3 inferred from a sea-level
686 analysis of sedimentary core records in the Yellow River Delta. *Quaternary Science Reviews*, 152, 72-79.

687 Pirazzoli, P.A., 2005. Marine terraces. In: Schwartz, M.L. (Ed.), *Encyclopedia of Coastal Science*. Springer
688 Netherlands, Dordrecht, pp. 632-633.

689 Railsback, L. B., Gibbard, P. L., Head, M. J., Voarintsoa, N. R. G., & Toucanne, S. (2015). An optimized scheme of
690 lettered marine isotope substages for the last 1.0 million years, and the climatostratigraphic nature of isotope stages
691 and substages. *Quaternary Science Reviews*, 111, 94-106.

692 Regard, V., Pedoja, K., De La Torre, I., Saillard, M., Corte_s-Aranda, J., Nexer, M., 2017. Geometrical trends within
693 sequences of Pleistocene marine terraces: selected examples from California, Peru, Chile and New-Zealand.
694 *Zeitschrift Fur Geomorphologie* 61 (1), 53e73.

695 Roberts, G. P., Houghton, S. L., Underwood, C., Papanikolaou, I., Cowie, P. A., van Calsteren, P., ... & McArthur, J.
696 M. (2009). Localization of Quaternary slip rates in an active rift in 105 years: An example from central Greece
697 constrained by ²³⁴U-²³⁰Th coral dates from uplifted paleoshorelines. *Journal of Geophysical Research: Solid Earth*,
698 114(B10).

699 Roberts, D. L., Karkanas, P., Jacobs, Z., Marean, C. W., & Roberts, R. G. (2012). Melting ice sheets 400,000 yr ago
700 raised sea level by 13 m: Past analogue for future trends. *Earth and Planetary Science Letters*, 357, 226-237.

701 Roeser, P., Franz, S. O., & Litt, T. (2016). Aragonite and calcite preservation in sediments from Lake Iznik related to
702 bottom lake oxygenation and water column depth. *Sedimentology*, 63(7), 2253-2277.

703 Rosenbloom, N. A., & Anderson, R. S. (1994). Hillslope and channel evolution in a marine terraced landscape, Santa
704 Cruz, California. *Journal of Geophysical Research: Solid Earth*, 99(B7), 14013-14029.

705 Rovere, A., Raymo, M. E., Vacchi, M., Lorscheid, T., Stocchi, P., Gomez-Pujol, L., ... & Hearty, P. J. (2016). The
706 analysis of Last Interglacial (MIS 5e) relative sea-level indicators: Reconstructing sea-level in a warmer world. *Earth-
707 Science Reviews*, 159, 404-427.

708 Rovere, A., Ryan, D. D., Vacchi, M., Dutton, A., Simms, A. R., & Murray-Wallace, C. V. (2023). The World Atlas
709 of Last Interglacial Shorelines (version 1.0). *Earth System Science Data*, 15(1), 1-23.

710 Schellmann, G., & Radtke, U. (2004). A revised morpho- and chronostratigraphy of the Late and Middle Pleistocene
711 coral reef terraces on Southern Barbados (West Indies). *Earth-Science Reviews*, 64(3-4), 157-187.

712 Shakun, J. D., Lea, D. W., Lisiecki, L. E., & Raymo, M. E. (2015). An 800-kyr record of global surface ocean $\delta^{18}O$
713 and implications for ice volume-temperature coupling. *Earth and Planetary Science Letters*, 426, 58-68.

714 Siddall, M., Smeed, D. A., Hemleben, C., Rohling, E. J., Schmelzer, I., & Peltier, W. R. (2004). Understanding the
715 Red Sea response to sea level. *Earth and Planetary Science Letters*, 225(3-4), 421-434.

716 Sondi, I., & Juračić, M. (2010). Whiting events and the formation of aragonite in Mediterranean Karstic Marine Lakes:
717 new evidence on its biologically induced inorganic origin. *Sedimentology*, 57(1), 85-95.

718 Spratt, R. M., & Lisiecki, L. E. (2016). A Late Pleistocene sea level stack. *Climate of the Past*, 12(4), 1079-1092.

719 Stein, M., Torfstein, A., Gavrieli, I., & Yechieli, Y. (2010). Abrupt aridities and salt deposition in the post-glacial
720 Dead Sea and their North Atlantic connection. *Quaternary Science Reviews*, 29(3-4), 567-575.

721 Stirling, C. H., Esat, T. M., Lambeck, K., McCulloch, M. T., Blake, S. G., Lee, D. C., & Halliday, A. N. (2001).
722 Orbital forcing of the marine isotope stage 9 interglacial. *Science*, 291(5502), 290-293.

723 Strobl, M., Hetzel, R., Fassoulas, C., & Kubik, P. W. (2014). A long-term rock uplift rate for eastern Crete and
724 geodynamic implications for the Hellenic subduction zone. *Journal of Geodynamics*, 78, 21-31.

725 Sunamura, T. (1992). *Geomorphology of Rocky Coasts*, vol. 3. John Wiley & Son Ltd.

726 Tawil-Morsink, K., Austermann, J., Dyer, B., Dumitru, O. A., Precht, W. F., Cashman, M., ... & Raymo, M. E. (2022).
727 Probabilistic investigation of global mean sea level during MIS 5a based on observations from Cave Hill, Barbados.
728 *Quaternary Science Reviews*, 295, 107783.

729 Toomey, M., Ashton, A. D., & Perron, J. T. (2013). Profiles of ocean island coral reefs controlled by sea-level history
730 and carbonate accumulation rates. *Geology*, 41(7), 731-734.

731 Van Daele, M., van Welden, A., Moernaut, J., Beck, C., Audemard, F., Sanchez, J., ... & De Batist, M. (2011).
732 Reconstruction of Late-Quaternary sea- and lake-level changes in a tectonically active marginal basin using seismic
733 stratigraphy: The Gulf of Cariaco, NE Venezuela. *Marine Geology*, 279(1-4), 37-51.

734 Waelbroeck, C., Labeyrie, L., Michel, E., Duplessy, J. C., Mcmanus, J. F., Lambeck, K., ... & Labracherie, M. (2002).
735 Sea-level and deep water temperature changes derived from benthic foraminifera isotopic records. *Quaternary science*
736 *reviews*, 21(1-3), 295-305.

737 Watkins, S. E., Whittaker, A. C., Bell, R. E., McNeill, L. C., Gawthorpe, R. L., Brooke, S. A., & Nixon, C. W. (2019).
738 Are landscapes buffered to high-frequency climate change? A comparison of sediment fluxes and depositional
739 volumes in the Corinth Rift, central Greece, over the past 130 ky. *GSA Bulletin*, 131(3-4), 372-388.

740 Weber, G.E. (1990). Late Pleistocene slip rates on the San Gregorio fault zone at Point Ano Nuevo, San Mateo County,
741 California, in Garrison, R.E., et al., eds., *Geology and tectonics of coastal California, San Francisco to Monterey*
742 (volume and guidebook): Bakersfield, California, Pacific Section, American Association of Petroleum Geologists, p.
743 193-203.

744 Webster, J. M., Wallace, L. M., Clague, D. A., & Braga, J. C. (2007). Numerical modeling of the growth and drowning
745 of Hawaiian coral reefs during the last two glacial cycles (0-250 kyr). *Geochemistry, Geophysics, Geosystems*, 8(3).
746